iScience

CellPress
OPEN ACCESS

Article

Ultra-large scale virtual screening identifies a small molecule inhibitor of the Wnt transporter Wntless

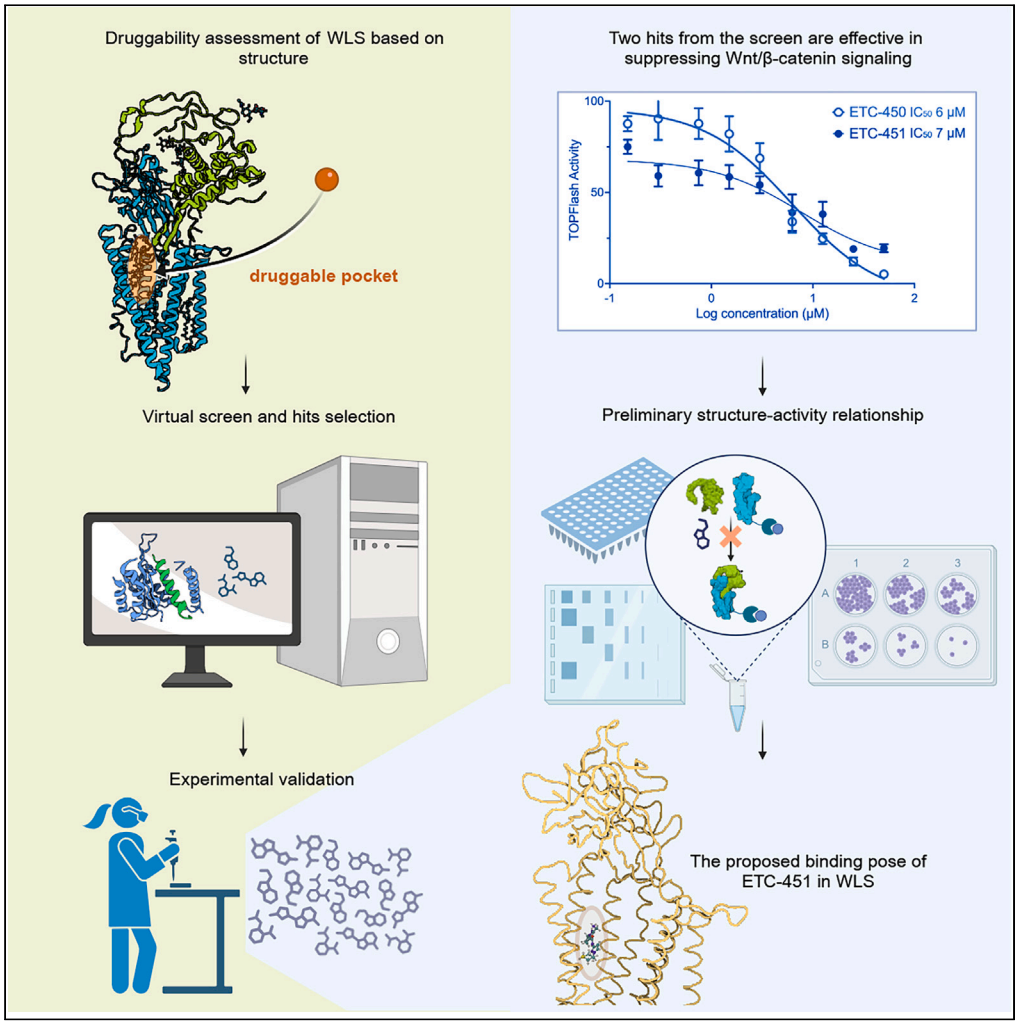

Jia Yu, Pei-Ju Liao, Thomas H. Keller, Joseph Cherian, David M. Virshup, Weijun Xu

david.virshup@duke-nus.edu.sg (D.M.V.)
xu_weijun@eddc.sg (W.X.)

Highlights

WLS is an essential WNT transporter with a GPCR pocket but it has not been drugged

Ultra-large scale virtual screening informed cell-based testing of WLS inhibitors

We identify ETC-451 as a first-in-class hit that blocks Wnt interaction with WLS

ETC-451 provides a structural template for small molecule drug design targeting WLS

Yu et al., iScience 27, 110454
August 16, 2024
https://doi.org/10.1016/j.isci.2024.110454

iScience

CellPress
OPEN ACCESS

Article

Ultra-large scale virtual screening identifies a small molecule inhibitor of the Wnt transporter Wntless

Jia Yu,[1,4,5] Pei-Ju Liao,[1,5] Thomas H. Keller,[2] Joseph Cherian,[2] David M. Virshup,[1,3,6,*] and Weijun Xu[2,7,*]

SUMMARY

Wnts are lipid-modified glycoproteins that play key roles in both embryonic development and adult homeostasis. Wnt signaling is dysregulated in many cancers and preclinical data shows that targeting Wnt biosynthesis and secretion can be effective in Wnt-addicted cancers. An integral membrane protein known as Wntless (WLS/Evi) is essential for Wnt secretion. However, WLS remains undrugged thus far. The cryo-EM structure of WLS in complex with WNT8A shows that WLS has a druggable G-protein coupled receptor (GPCR) domain. Using Active Learning/Glide, we performed an ultra-large scale virtual screening from Enamine's REAL 350/3 Lead-Like library containing nearly 500 million compounds. 68 hits were examined after on-demand synthesis in cell-based Wnt reporter and other functional assays. ETC-451 emerged as a potential first-in-class WLS inhibitor. ETC-451 blocked WLS-WNT3A interaction and decreased Wnt-addicted pancreatic cancer cell line proliferation. The current hit provides a starting chemical scaffold for further structure or ligand-based drug discovery targeting WLS.

INTRODUCTION

Wnt signaling pathways are important throughout the animal kingdom to regulate cellular growth and tissue communication.[1,2] Upon the binding of Wnt ligands to their receptors and coreceptors, a cascade of intracellular signaling events occurs (Figure 1) that results in the tissue-specific transcriptional regulation of multiple genes that regulate biological processes involved in proliferation and differentiation.[3] Deregulation of the Wnt pathway results in cancers, fibrosis, immune suppression, and degenerative diseases in humans (reviewed in[4–6]). Due to its importance in controlling cell proliferation, the discovery and development of inhibitors capable of perturbing Wnt signaling is an area of extensive research in both academia and industry.

Both Wnt biogenesis and downstream signaling pathways offer several druggable targets. Wnt proteins are post-translationally modified during their biosynthesis.[7,8] A mono-unsaturated palmitoleate is attached to a highly conserved serine residue on Wnt by an endoplasmic reticulum (ER)-resident acyltransferase named Porcupine (PORCN).[7,9] This palmitoleation is essential for Wnt to subsequently bind to its transporter, the integral membrane protein Wntless (WLS, also called Evi) for secretion into the extracellular environment.[10–12] There, Wnt binds to its cognate receptor Frizzled as well as other coreceptors to initiate downstream signaling. One of the most studied signaling pathways is the β-catenin dependent pathway, focusing on the tightly regulated protein β-catenin that activates TCF-driven transcription. β-catenin levels are controlled by the multi-protein destruction complex that comprises both scaffold proteins as well as kinases. Many studies have aimed to find drugs that destabilize β-catenin or block the interaction between β-catenin and TCF or other transcription coactivators.[13,14] For the upstream Wnt synthesis and secretion, PORCN inhibitors have been identified in the past decade as potential therapeutics for Wnt-addicted tumors (reviewed in[15]). Several of these small molecules such as LGK974 and ETC-159 are currently undergoing clinical trials.[16–18] Another approach to inhibiting the Wnt pathway involves targeting the interaction between Wnt ligands and FZD receptors. Recombinant fusion proteins and antibodies that target FZDs are being developed as potential Wnt/FZD antagonists.[19,20] These inhibitors block the binding of Wnt ligands to FZD receptors, thereby disrupting downstream signaling. However, to date, no inhibitors have been reported to target WLS (Figure 1).

Recently the structures of the human WLS bound to WNT8A and WNT3A have been determined by single particle cryo-electron microscopy.[21,22] Although bound to different Wnt ligands, these complexes showed very similar WLS structures. WLS contains an amino-terminal transmembrane helix followed by a large extracellular globular domain and then a G-protein coupled receptor (GPCR)-related transmembrane domain consisting of an additional seven helices. WLS has extensive interactions with the Wnt ligand, and the bound palmitoleate

[1]Programme in Cancer and Stem Cell Biology, Duke-NUS Medical School, Singapore 169857, Singapore
[2]Experimental Drug Development Centre, 10 Biopolis Road, Chromos, Singapore 138670, Singapore
[3]Department of Pediatrics, Duke University School of Medicine, Durham, NC 27710, USA
[4]Present address: Pediatric Bone Marrow Transplant and Cell Therapy Center, KK Women's and Children's Hospital, Singapore 169856, Singapore
[5]These authors contributed equally
[6]Senior author
[7]Lead contact
*Correspondence: david.virshup@duke-nus.edu.sg (D.M.V.), xu_weijun@eddc.sg (W.X.)
https://doi.org/10.1016/j.isci.2024.110454

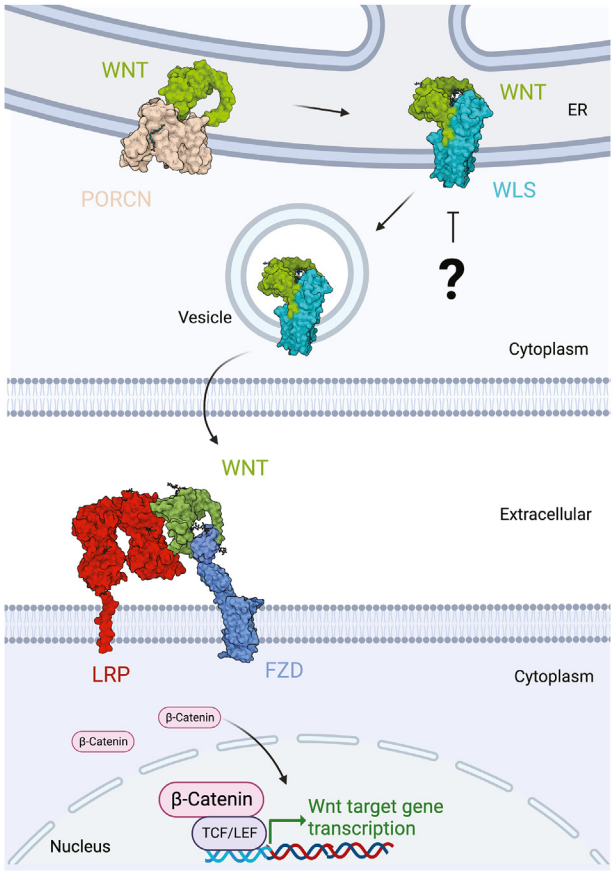

Figure 1. WLS is a dedicated and essential Wnt transporter

The cartoon illustrates critical proteins involved in the Wnt/β-catenin pathway, including the acyltransferase PORCN and the transporter WLS in the Wnt-producing cells. FZD and LRP5/6 in the signal-receiving cells signal to stabilize β-catenin, allowing it to drive gene expression. Surface models were derived from solved structures as follows: PORCN (PDB: 7URE), WNT (PDB: 7KC4), WNT-WLS complex (PDB: 7KC4), the LRPE1E2-WNT-FZD CRD complex (PDB: 8CTG) with FZD (PDB: 6WW2).

moiety is inserted deeply into the hydrophobic cavity of WLS (Figures 2A and 2B). Interestingly, structural homology searches and binding site detection analysis revealed that a druggable pocket may be present within the WLS transmembrane domain, similar to the canonical drug binding sites in other GPCRs.

Recently, *in silico* screening of compound libraries broadly covering expanded chemical space has gained increasing attention in the drug discovery pipeline. Since 2019, ultra-large virtual screening has been reported to contribute toward improved hit identification. Lyu et al. used 1500 CPU cores to dock 138 million compounds in the dopamine D_4 receptor and tested 549 make-on-demand molecules, among which 83 compounds showed K_i ranging from 18.4 nM to 8.3 μM with a hit rate of 22%.[25] In the same study, the authors docked 99 million compounds (1500 CPU cores) in the AmpC β-lactamase and tested 44 compounds. 5 of them had K_i values ranging from 1.3 to 400 μM (hit rate 11%). Gorgulla et al. docked 1.3 billion compounds (average 8000 CPU cores) in the KEAP1 redox sensor and cherry-picked 590 compounds for experimental testing, resulting in 69 hits confirmed as binders by surface plasmon resonance (SPR).[26] Carlsson et al. conducted structure-based docking to screen a diverse library of 235 million virtual compounds (3500 CPU cores) against the active site of the 3CLpro protease of SARS-CoV2.[27] Three inhibitors were identified out of 100 top-ranked compounds from binding and enzymatic assays. Kirtrich et al. proposed a "virtual synthon hierarchical enumeration screening" (V-SYNTHES) approach that performs docking calculations on a focused set of fragment compounds that are representative of all the scaffolds available for library synthesis and the corresponding reagents to elaborate them.[28] The approach was applied to discover new chemotypes for cannabinoid receptor CB2 antagonists and achieved a hit rate of 23% for submicromolar ligands, exceeding the hit rate of standard virtual screening, while taking about 100 times less computational resources. Thus, modern virtual screening is proving effective at generating promising chemical hits.

To develop novel inhibitors of Wnt signaling, we sought to target the dedicated carrier protein WLS, which has a potentially druggable site within the transmembrane bundle. We initiated an ultra-large scale virtual screening campaign using the Enamine make-on-demand lead-like (350/3) library containing about 500 million compounds. We selected a diverse set of 86 compounds for synthesis. All the successfully synthesized compounds were tested using Wnt reporter assay as the primary readout. ETC-451 showed the inhibition of Wnt-WLS binding and

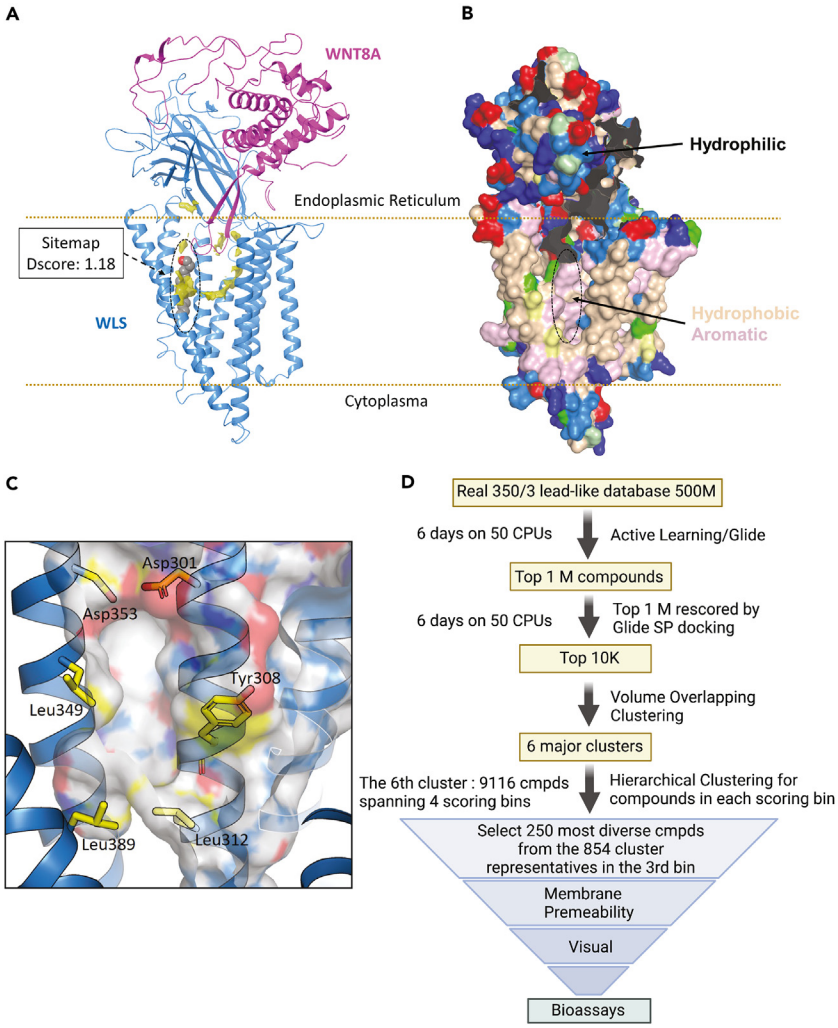

Figure 2. Sitemap identifies a potential druggable pocket in WLS amenable to small molecule discovery via virtual screening

(A) Binding site detection within the WLS transmembrane domain identifies site 1 (black circle) as the most druggable pocket. WLS is in blue and WNT8A is in purple. WNT palmitoleate tail is in gray. (PDB: 7KC4)

(B) Surface representation of WLS, color-coded by the chemical properties of amino acids. Red: negatively charged; Blue: positively charged; Wheat: hydrophobic; Magenta: aromatic; and Green: Glycine.

(C) Focused pocket view of the identified druggable site in surface representation with WLS transmembrane helices in blue ribbon.

(D) Virtual screening and hit selection workflow. Volume overlapping clustering was performed using Schrödinger Maestro.[23] Within the largest cluster (6th cluster), the 3rd bin contains 7441 compounds and covers 854 chemical fingerprint-based subclusters. Using diversity-based selection, 250 compounds were further selected. To this dataset, membrane permeability was applied to the filter using a cutoff −5.2 based on LogPermRRCK value.[24] Finally, a list of 86 diverse compounds was shortlisted as virtual hits for Enamine synthesis.

downregulated Wnt target gene expression as well as cell proliferation in Wnt-sensitive pancreatic cell lines. To our knowledge, this is the first study to report a large scale *in silico* computational screen leading to the identification of the first WLS inhibitor, providing a starting template for further medicinal chemistry efforts to improve the current hit compound. In addition, here we release the top 10,000 ranked hits from our virtual screening that provides a plethora of chemical information for drugging WLS as a collective effort from the Wnt community (see STAR methods).

RESULTS

Virtual screening of enamine "350/3" lead-like library

Using the previously solved WNT8A-WLS complex,[21] we asked whether a potential druggable binding site that is amenable to small molecule binding is present in WLS. To probe this, we first removed WNT8A from the complex structure and calculated the top 5 binding sites using Sitemap (Schrödinger). Interestingly, Site 1 (Figure 2A, black circle), which aligned with the GPCR drug binding site, was identified as the most druggable pocket within the TM tunnel of WLS. Notably, the pocket features partially polar residues at the top with predominantly hydrophobic

residues lining the lower pocket (Figures 2B and 2C). Next, we performed a virtual screen using the Enamine 350/3 Lead-like library containing compounds with the most stringent physicochemical profiles to have high potency for optimization: 270 ≤ MW ≤ 350, 14 ≤ HAC ≤ 26, SlogP ≤ 3, and aryl rings ≤ 2. During the virtual screening, we implemented default settings from Active Learning/Glide (Schrödinger) (see STAR methods for details). As briefly illustrated in Figure 2D, a random diversity based subset (50K) of the ligand library was selected and docked with Glide SP mode.[29] The docking scores of this subset were used to train a DeepChem learning model,[30] which was subsequently used to predict docking scores across the entire ligand database. This was followed by another 2 rounds of active learning (Figure S1A), where an attempt was made to improve the model by selecting the top scoring compounds to form the focus for the final stage of Glide SP rescoring.

Our virtual screening was performed on a 128-CPU cluster. We implemented a 50-parallel CPU job for Glide SP docking and the DeepChem learning was performed using one NVIDIA V100 Tensor core GPU. Upon the completion of Active Learning/Glide, the top 1 million ligands, as predicted by the active learning, were rescored by Glide SP docking. We focused our post-virtual screening hit selection on the top 10,000 ranked compounds based on the Glide SP scores. From this list, the unique compounds were saved. Next, volume overlapping clustering was applied to classify compounds based on the volume occupancy within the binding site, resulting in 6 major clusters within the top 10,000 virtual hits. We then visually inspected the binding poses of compounds from each cluster. The largest cluster, containing 9116 compounds, appeared the most attractive due to the best mutual fitness between the shape of the binding pocket and the ligands. In addition, we used the Schrödinger "membrane permeability" module to shortlist compounds.[24] Aided by visual inspection for putative protein-ligand interactions, a total of 86 diverse (Figure S1B) REAL compounds were selected and ordered for synthesis from Enamine.[31]

ETC-450 and ETC-451 reduced Wnt secretion and reporter activity

We tested 68 successfully synthesized make-on-demand compounds *in vitro* using a well-established Wnt/β-catenin reporter assay.[10,17] STF3A cells are HEK293 cells with an integrated WNT3A expression construct and β-catenin responsive SuperTOPFlash (STF) luciferase reporter. These Wnt-high reporter cells were treated with individual inhibitors for 48 h and then luciferase activity was measured (Figure 3A). Since WLS inhibitors block Wnt signaling by inhibiting Wnt secretion, the addition of exogenous Wnt ligands should rescue the downstream reporter activity. Therefore, we also tested the compounds using STF reporter cells (lacking endogenous WNT3A) cultured with WNT3A-conditioned medium for comparison (Figures 3B and 3C). 2 out of 68 compounds, ETC-2188450 and ETC-2188451 (henceforth referred to as ETC-450 and -451) were found to selectively inhibit signaling in STF3A cells, but not in STF cells stimulated with WNT3A-conditioned medium (Figures 3A–3C). ETC-451 also did not block signaling resulting from downstream stimuli including activated LRP6 (ΔN-LRP6), stabilized β-catenin (β-catenin S45A mutant)and a GSK3 inhibitor BIO,[32] confirming it is a specific WLS inhibitor (Figure S2). Both compounds exhibited a dose-dependent inhibition of Wnt/β-catenin reporter activity with IC_{50}s of 6.3 μM and 7.7 μM, respectively (Figure 3A).

Additionally, we collected the cell culture medium from ETC-450 and ETC-451 treated STF3A cells to test if the secretion of WNT3A into the media is reduced. Although not as potent as the PORCN inhibitor ETC-159, WNT3A secretion was significantly reduced in a dose-dependent manner after treatment with ETC-450 and ETC-451 (Figures 3D and 3E). The results indicated that the two hits are potential WLS inhibitors and were, therefore, further characterized.

ETC-451 blocks the interaction of Wnt with Wntless

Since the potential drug binding pocket used for the virtual screening is also where the Wnt-palmitoleate moiety binds, the binding of the small molecules could in theory competitively inhibit the binding of Wnt to WLS. To test this hypothesis, we performed co-immunoprecipitation assays (CoIP) to examine the effect of the compounds on the interaction between WNT3A and V5-epitope tagged WLS. Indeed, ETC-451 diminished the binding of WNT3A to WLS, consistent with the proposed mechanism of action (Figures 4A and 4B). Conversely, ETC-450 did not block Wnt binding to WLS, suggesting a distinct mode of inhibition for this compound.

As an additional test of specificity, we examined the effect of the hits on the Wnt-PORCN interaction (Figure 4C). PORCN inhibitors including LGK974 and ETC-159 prevent the binding of palmitoleoyl-CoA to the enzyme PORCN and therefore directly block the interaction of PORCN and Wnt.[33,34] In our hands, ETC-159 but not ETC-450 nor ETC-451 blocked the binding of WNT3A and PORCN. Thus, ETC450 and ETC-451 do not appear to be PORCN inhibitors (Figure 4C). In addition, we observed an unexpected reduction of WNT3A protein levels in the lysate upon ETC-451 but not ETC-159 treatment, especially at high concentrations (See normalized WNT3A level quantification for Figures 3E, 4A, and 4C). We suspect that lipidated WNT may be more prone to denaturation and degradation than non-palmitoleated WNT in the absence of WLS binding.

To further validate that WLS is the target of the compounds, we tested whether over-expression of WLS can rescue the inhibition of Wnt/β-catenin reporter activity upon the treatment of compounds. Indeed, when a low concentration of the compounds (close to the IC50) was used, over-expression of WLS but not PORCN reversed the inhibitory effects of ETC-450 and ETC-451 on the Wnt/β-catenin reporter activities. In a control experiment, over-expression of PORCN rescued the PORCN inhibitor ETC-159's activity in suppressing the reporter assay (Figure 4D). Taken together, these data suggest that both ETC-450 and ETC-451 are potential WLS-specific inhibitors.

ETC-451 reduced Wnt target gene expression and colony formation in Wnt sensitive pancreatic cells

Because of its ability to block the Wnt-WLS interaction, we focused on ETC-451 and examined its effect on the downstream Wnt signaling pathway. We compared the effect of ETC-451 on Wnt target gene expression and colony forming ability in Wnt-addicted HPAF-II and Wnt-independent PANC 08.13 pancreatic cancer cell lines (Figure 5).[35] The Wnt target genes *AXIN2* and *RNF43* are highly expressed in HPAF-II cells but not in PANC 08.13 cells. ETC-451 treatment reduced both *AXIN2* and *RNF43* expression in a dose-dependent manner in the Wnt-high HPAF-II cells but not in the Wnt-low PANC 08.13 cells (Figure 5A). Wnt inhibition in Wnt-addicted cancers also causes the

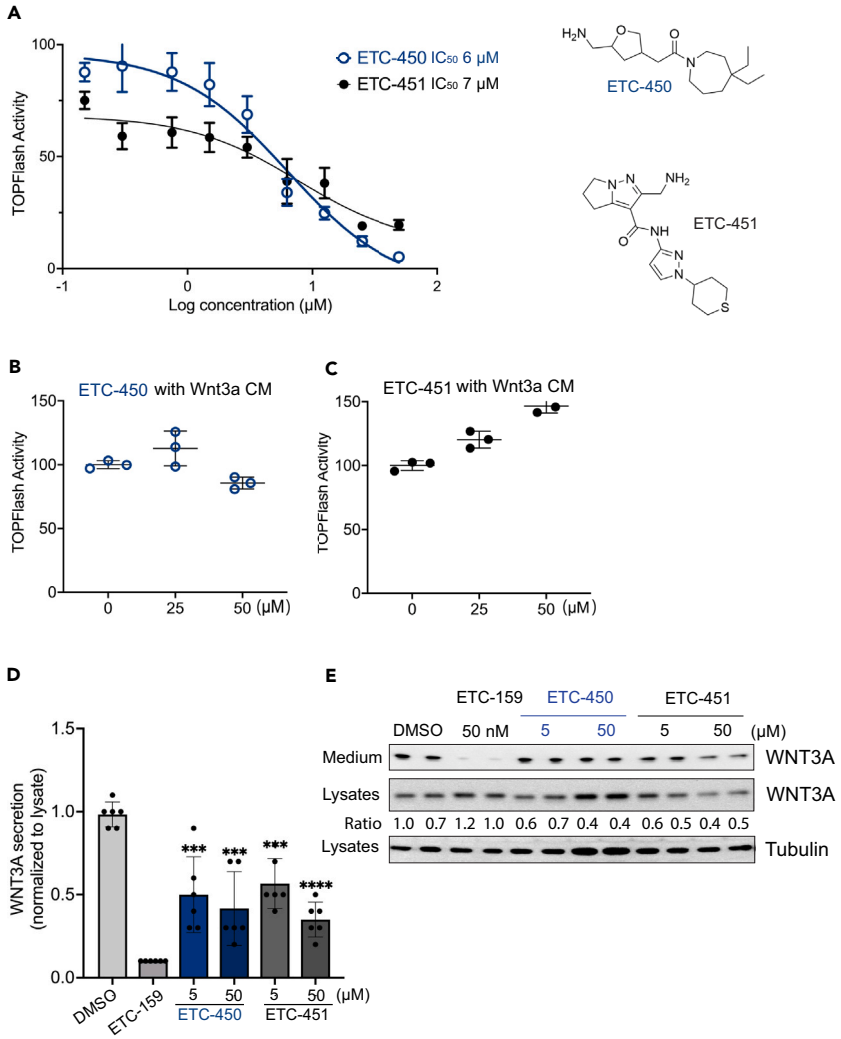

Figure 3. Two hits from the WLS inhibitor screen are effective in suppressing Wnt/β-catenin signaling and WNT3A secretion

(A) Wnt/β-catenin reporter activity in STF3A cells was suppressed by 48 h treatment with the indicated concentration of ETC-450 or ETC-451. Luciferase activity was normalized to DMSO control. The chemical structures of ETC-450 and ETC-451 are shown on the right. Data are displayed as mean ± standard deviation (s.d.) and show one representative of three independent experiments with three biological replicates.

(B and C) WLS inhibitors do not suppress signaling stimulated by WNT3A-conditioned medium (CM). STF cells were co-cultured with WNT3A-conditioned medium and treated with ETC-450 or ETC-451 for 48 h, followed by the measurement of luciferase activity. Luciferase activity was normalized to DMSO control. Data are displayed as mean ± s.d. and show one representative of three independent experiments with three biological replicates.

(D and E) WLS inhibitors decrease WNT3A protein secretion. WNT3A protein levels in the culture supernatants and lysates of STF3A cells treated with the compounds were assessed by immunoblotting. As a control, the PORCN inhibitor ETC-159 was used at 50 nM. The ratio represents the relative quantification of WNT3A levels in the lysates, normalized to tubulin. The significance of the difference was assessed by unpaired *t*-test comparing each compound's treatment with DMSO. The mean ± s.d. is shown for the data from three independent experiments each with two replicates. ***, $p < 0.001$; ****, $p < 0.0001$.

upregulation of differentiation markers such as *MUC4*.[17] ETC-451 increased *MUC4* expression in the Wnt-addicted HPAF-II cells, but not in the Wnt-independent PANC 08.13 cells (Figure 5A).

We similarly measured the effects of the putative WLS inhibitor on colony formation in HPAF-II and PANC 08.13 cells. In HPAF-II cells, similar to the effects of the PORCN inhibitor ETC-159, ETC-451 suppressed colony formation in a dose dependent manner. Neither the PORCN inhibitor nor ETC-451 suppressed colony formation in the Wnt-independent PANC 08.13 cells (Figures 5B and 5C). Thus, ETC-451 appears to act on transcription and proliferation in a Wnt specific manner.

ETC-451 analogs retain Wnt inhibition activities and revealed preliminary structure-activity relationship for Wntless inhibition

To establish a structure-activity relationship (SAR) of ETC-451 derivatives, we ordered 11 analogs with the same dihydro-pyrrolo pyrazole core scaffold and examined their ability to inhibit the Wnt/β-catenin reporter activity (Figure S3A). The assay results suggested

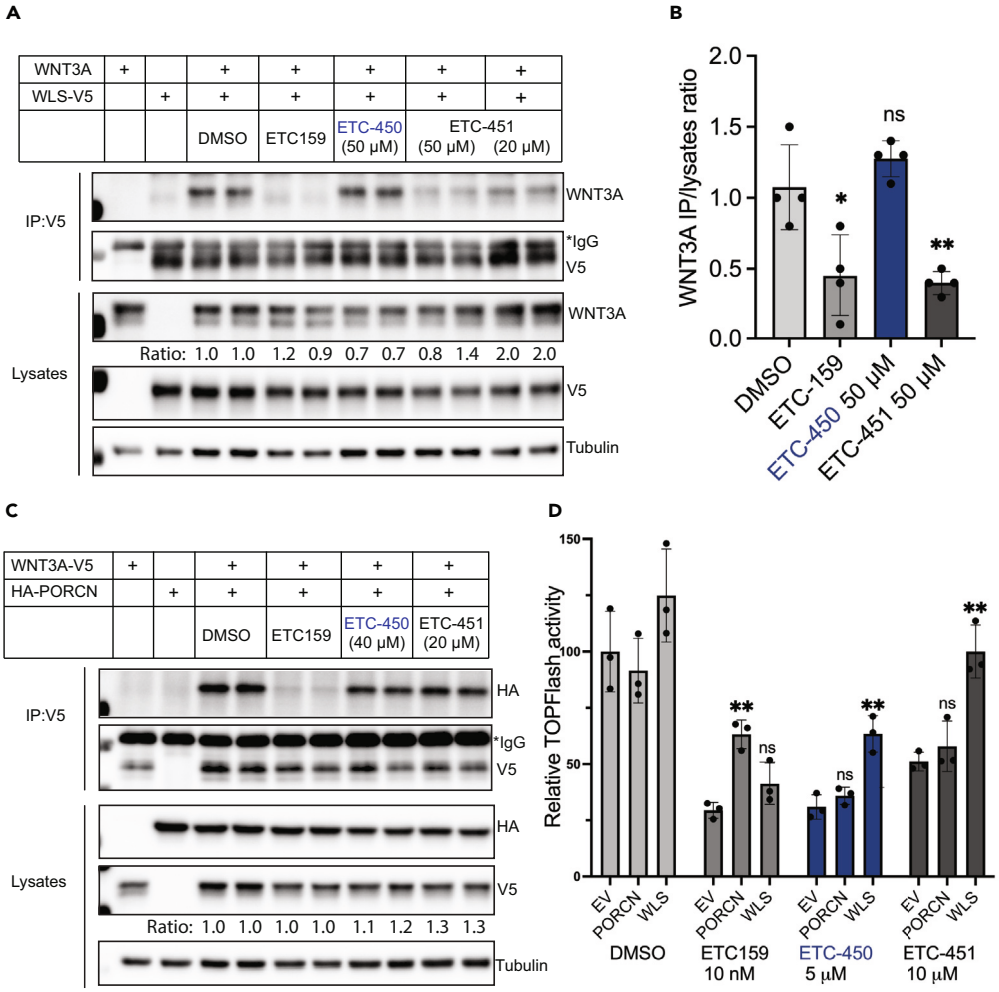

Figure 4. The WLS inhibitor ETC-451 blocks the interaction of WNT3A and WLS

(A and B) STF cells were treated with the indicated compounds for 48 h, and the co-immunoprecipitation of WNT3A and WLS-V5 was performed. Representative immunoblots are shown in (A) and results from two independent experiments are quantified in (B). ETC-159 was used at 50 nM. The ratio represents the relative quantification of WNT3A levels in the lysates, normalized to tubulin. The significance of the difference from the DMSO control was assessed by unpaired *t*-test. The mean ± s.d. is shown for (B) from two independent experiments each with two replicates. *, $p < 0.05$; **, $p < 0.01$.

(C) The binding of WNT3A to PORCN was not affected by either ETC-450 or ETC-451. The ratio represents the relative quantification of V5-tagged WNT3A levels in the lysates, normalized to tubulin.

(D) The inhibitory effect of ETC-451 on ***β***-catenin reporter activity was rescued by overexpression of WLS. STF cells were transfected with WNT3A, WLS, and PORCN expression plasmids as indicated, treated with the indicated compounds for 48 h, and reporter activity was measured. Data were analyzed using unpaired *t*-test corrected for multiple comparisons. ETC159 was in 10 nM treatment as a positive control to abolish the binding of WNT3A and WLS entirely. The significance of the difference was assessed by unpaired *t*-test comparing each plasmid with EV (empty vector). The mean ± s.d. is shown for three replicates represented from three independent experiments. **, $p < 0.01$.

that the 2-aminomethyl group on the dihydro-pyrrolo pyrazole is important, as the four close analogs (ETC-451H to ETC-451K) that do not contain the moiety were inactive in the reporter assay (Data not shown). On the other hand, compound ETC-451A, which retains the 2-aminomethyl but has a benzyl group attached to the central pyrazole ring shows a similar IC_{50} as ETC-451 (Figure 6A). We chose ETC-451A for further characterization. In a co-immunoprecipitation assay, ETC-451A reduced the WNT3A-WLS interaction similar to the parental ETC-451. In contrast, an analog of ETC-450, ETC-450A (Figure S3B), did not inhibit the interaction (Figure 6B). ETC-451A also decreased Wnt target gene (*AXIN2* and *RNF43*) expression and increased differentiation marker *MUC4* expression in Wnt-sensitive HPAF II cells but not Wnt-independent PANC 08.13 cells (Figure 6C). Importantly, like ETC-451, ETC-451A at 25 μM inhibited the colony formation of the Wnt-dependent HPAF-II cells but not the Wnt-independent PANC 08–13 cells (Figures 6D and 6E).

To gain insights into how ETC-451 and its active analogs interact with WLS (PDB: 7KC4) at the molecular level, we revisited the predicted binding mode of ETC-451 from the virtual screening generated pose (Figure 7A). Next, we performed a docking experiment by

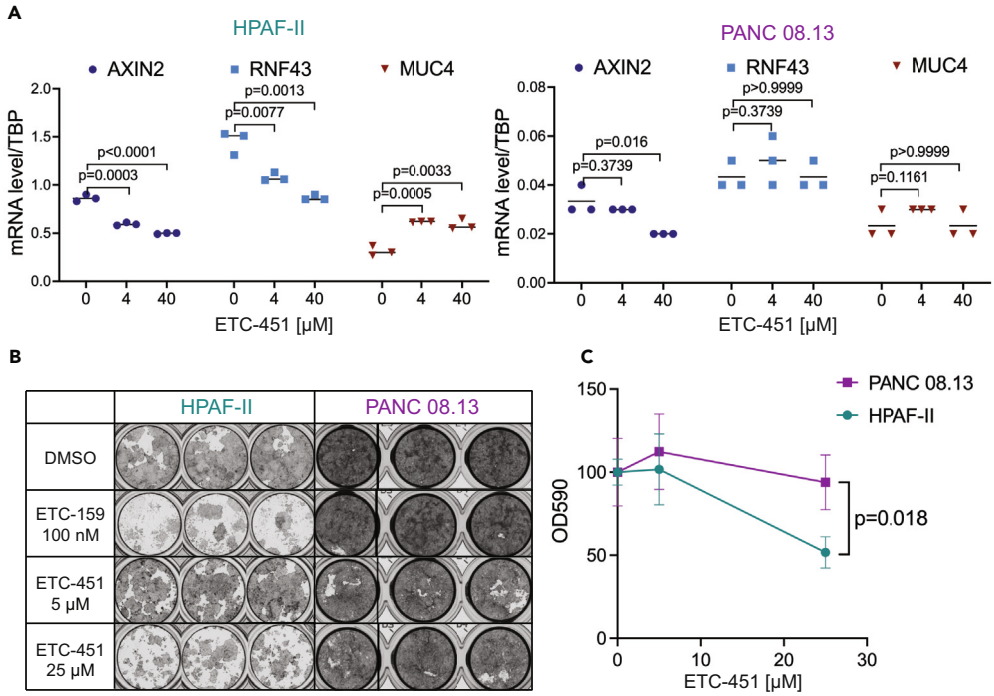

Figure 5. The effect of ETC-451 is specific to Wnt-regulated genes and cells

(A) The transcript abundance of the indicated Wnt-regulated genes was determined by RT-qPCR in Wnt-addicted HPAF-II and Wnt-independent PANC 08.13 cells after 72 h of ETC-451 treatment. The significance of the difference from the DMSO control was assessed by unpaired *t*-test. The mean is shown for the three replicates.

(B) HPAF-II and PANC 08.13 cells were seeded at low density in a 48-well plate and treated with ETC-451 or ETC-159 for 2 to 3 weeks. The cell density was quantified by crystal violet staining (OD590) shown in (C). The significance of the difference between HPAF-II and PANC 08.13 with ETC-451 25 μM treatment was assessed by unpaired *t*-test. The mean ± s.d. is shown for (C) represents the average of three biological replicates.

sampling possible binding modes of the active analogs in the druggable binding pocket that was used for the virtual screening (Figure 7B). The hit ETC-451 and its active analogs were predicted to sit vertically within the targeted site. Of note, the 2-aminomethyl group from the dihydro-pyrrolo pyrazole primarily formed polar interactions with the two acidic residues (Asp301 and Asp353) atop the binding site, providing a possible rationale that echoes our preliminary SAR suggesting the indispensable role of the 2-aminomethyl for interaction with WLS (Figure 7C). The amide linker was not simulated to form any polar interaction with the protein residues but rather directed the hydrophobic end of the inhibitors deeply through the lower binding pocket. The central pyrazole moiety was wedged in between Tyr308 and Leu349, whereas the thiane group made hydrophobic contacts with Leu312, Leu349, and Leu389. Interestingly, the dihydro-pyrrolo pyrazole core sandwiched in between TM4 and TM5 and tilted in a similar orientation to that of the palmitoleoyl tail from WNT3A, partially overlapping with the lipid upon superimposition (Figures 7A–7C). This provides a potential explanation for why ETC-451 blocks the WLS-WNT interaction.

As a further validation of the docking model, we performed 1-μs molecular dynamic (MD) simulations for the docked complex of ETC-451 and WLS. The simulation results showed that the protein-ligand interaction was stabilized throughout the whole simulation period with small Root-Mean-Square Deviation (RMSD) values (Figure S4A). The Root-Mean-Square Fluctuation (RMSF) was used to evaluate the flexibility of the ligand, and the average fluctuation in ETC-451 was from 0.8 to 1.1 Å (Figure S4B). MD simulations further revealed that Gly305 may form a hydrogen-bond contact with the amide NH from ETC-451, an interaction that was not predicted directly from docking (Figures 7D, S4C, and S4D). Moreover, Tyr308 formed intermittent pi-stacking interaction with the central pyrazole ring from the inhibitor (Figure 4C). Consistent with the docking, Asp301 and Asp353 interacted with the inhibitor extensively via H-bond interactions and salt bridges (Figures 7C, S4C, S4D, and Video S1). From the MD simulated trajectories, we also speculated that the pocket featuring the ligand-protein interactions was stable. As measured by RMSF of key residues enclosing the ligand binding pocket (Table S1), we show that the residues generally adopted little fluctuation for their side chains, indicating that throughout the whole MD simulation, the binding pocket was overall stabilized by the ligand binding. Further, we sampled 10 snapshots of the simulated structures and analyzed the binding site using SiteMap (Figure S5). The overall size and physicochemical features of the pockets were generally consistent across the sample structures. Finally, we also calculated the strength of protein-ligand interactions via the trajectory using per residue contribution in two aspects, namely van der Waals and electrostatic interactions. Asp301 and Asp 353 showed dominant contributions toward electrostatic binding (Table S2). Thus, the MD results are consistent with the modeling and docking predictions.

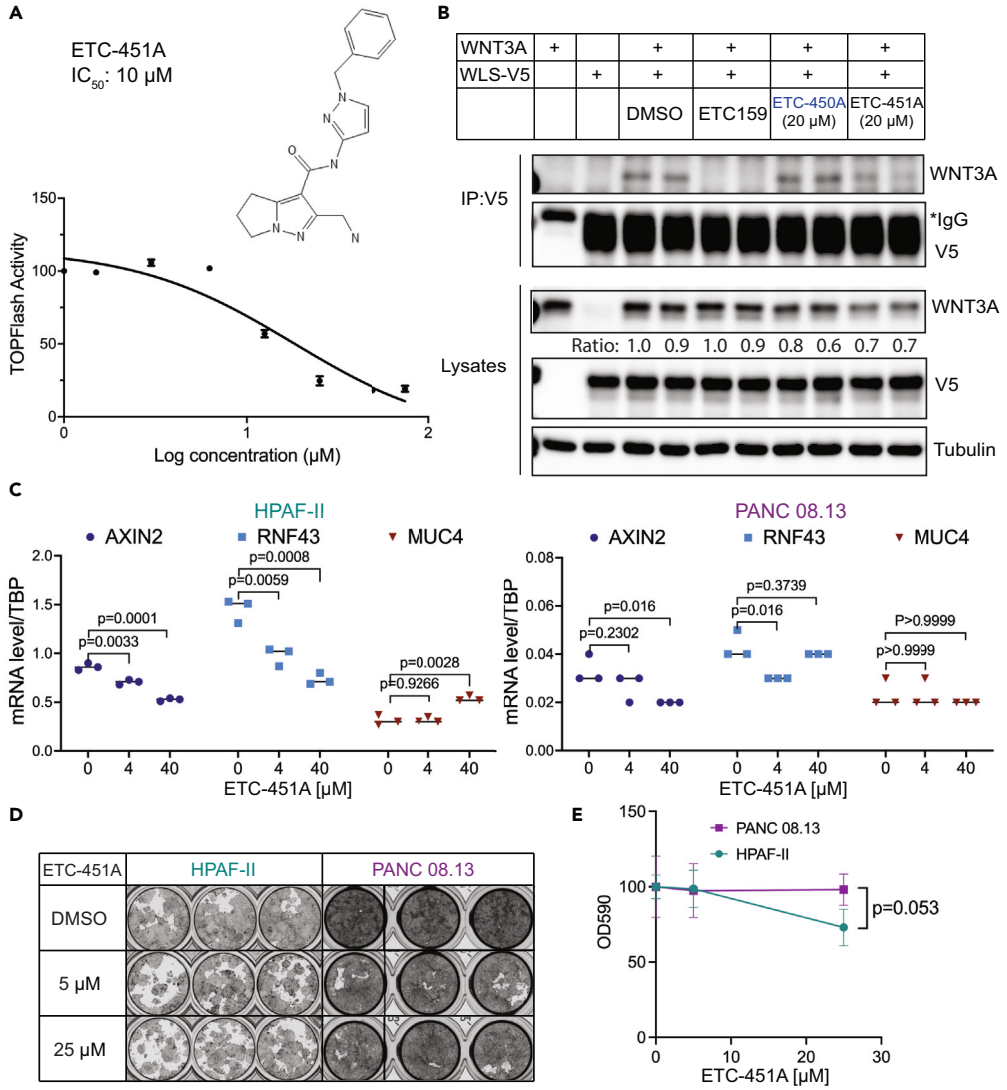

Figure 6. Initial structure-activity relationship of analogues of ETC-450 and ETC-451

(A) ETC-451A (an analogue of ETC-451) inhibits Wnt/β-catenin reporter activity of WNT3A. STF3A cells were treated with the indicated compounds for 48 h, and luciferase activity was measured. Data are displayed as mean ± s.d. and show one representative of three independent experiments with three biological replicates. The structure of ETC-451A is shown on the top panel.

(B) The effect of ETC-450A (an analogue of ETC-450) and ETC-451A on the interaction of WNT3A and WLS-V5. Cells co-expressing the indicated constructs were treated for 48 h before lysis and immunoprecipitation. The ratio represents the relative quantification of WNT3A levels in the lysates, normalized to tubulin.

(C–E) ETC-451A is also an effective inhibitor of Wnt function. Similar to Figure 5 but with ETC-451A. (C) regulation of Wnt-responsive genes in HPAF-II but not PANC 08.13 cells. The significance of the difference from the DMSO control was assessed by unpaired *t*-test. (D, E) inhibition of the colony formation of Wnt-addicted cells. The mean ± s.d. is shown for (E) represents the average of three biological replicates. The significance of the difference between HPAF-II and PANC 08.13 with ETC-451A 25 μM treatment was assessed by unpaired *t*-test.

To experimentally test our modeling results, we reasoned that mutating either Asp301 or Asp353 to alanine would affect the binding of the ETC-451, thus reducing its inhibitory potency and making WLS drug resistant. We tested this hypothesis using a previously described WLS knockout cell line that cannot secrete Wnt proteins and therefore does not have any Wnt reporter activity.[21,36] The re-expression of wild-type WLS in the cell line restores the Wnt reporter activity, and that activity can be inhibited by ETC-451 (Figure 7E, gray bars). The WLS D301A mutant was unstable and so was not tested further. Expression of D353A mutant WLS also restored Wnt reporter activity, and these cells were now resistant to ETC-451 treatment (Figure 7E, purple bars). Additionally, the interaction between the WNT3A and WLS D353A mutant was not affected by ETC-451, unlike the WT WLS (Figure S6). Notably, the D353A mutant, while it conferred resistance to ETC-451, did not confer resistance to ETC-450 nor to the PORCN inhibitor ETC-159 (Figure 7E). These results support the model that WLS residue Asp353 plays a critical role in ETC-451 binding. Taken together, the modeled binding pose of ETC-451 provided a mechanistic rationale for the experimental results showing that ETC-451 directly blocks Wnt-WLS interaction in the co-IP assay.

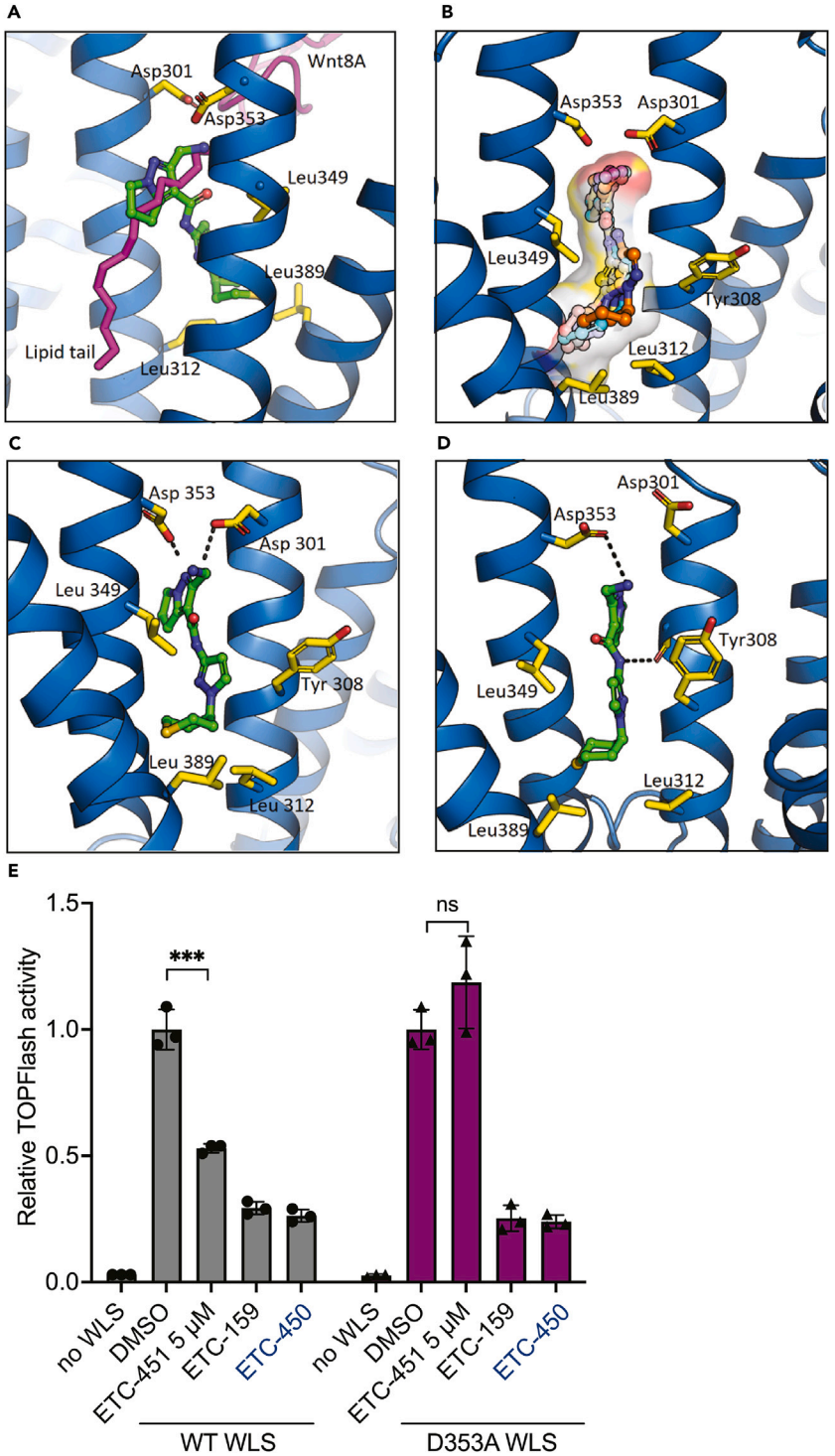

Figure 7. Proposed model of WLS inhibitor ETC-451 binding pose

(A) Lateral view of the docked pose of ETC-451 (in green stick representation), superimposed with the WNT8A-WLS complex (in purple stick representation). Note the conflict with the palmitoleate moiety.

(B) Docked poses of ETC-451 active analogues ETC-451A to ETC-451G. Stick represents the 7 analogues. The predicted drug binding cavity is in surface presentation.

(C) Docked pose of ETC-451 (in green stick representation) within the WLS transmembrane tunnel (blue ribbon represents WLS transmembrane helices). The 2-aminomethyl group formed polar interactions with WLS Asp301 and Asp353.

Figure 7. *Continued*

(D) MD simulation snapshot of ETC-451 illustrates the potential role of WLS Asp353 and Gly305. WLS residues colored in yellow; ETC-451 in green; WNT8A in purple; H-bond in black dotted line.

(E) WLS Asp353Ala mutant is resistant to inhibition by ETC-451. WLS knockout cells were transfected with SuperTOPFlash reporter, mCherry, WNT3A, and the indicated WLS expression plasmids. ETC-451 was added to cells after 6 h transfection, and reporter activity was assessed 24 h later. ETC-159 was used at 50 nM treatment and ETC-450 at 25 μM. The mean luciferase activities for DMSO treated conditions were normalized to 1. Data are displayed as mean ± s.d. and show one representative of three independent experiments with three biological replicates. ***, $p < 0.001$.

DISCUSSION

Wnt signaling is dysregulated in diverse disease states, and therefore considerable efforts have been made to develop effective inhibitors of the pathway. We report here the first small molecule inhibitor of WLS/Evi, the dedicated Wnt transporter. Using the recently solved cryo-EM structure and refined computer-aided modeling, we identified a druggable pocket in the GPCR domain of WLS and validated a hit through diverse cell-based assays. In addition, we performed an initial structure-activity relationship analysis and proposed the drug-WLS interaction model which was supported by the mutational analysis. This study represents a paradigm for modern computational drug discovery and provides new tools for targeting the Wnt pathway.

Computer aided drug discovery (CADD) was first developed in the 1970s and the first program for docking was available in the 1980s.[37,38] Although there were successful cases along the way, the overall confidence of applying CADD in early drug discovery remained an open question. In the last decade, the continuous improvement in force field development, sampling methods, and computational technologies brought about a revolutionary shift toward embracing computational approaches as a driving force for drug discovery. Indeed, today's computational chemistry plays roles spanning from the early phase of target identification and assessment for its druggability, hit/lead discovery via both structure and ligand based virtual screening, to the later phase of hit to lead campaign and lead optimization. For the stage of "hit discovery" *per se*, the field is entering an exciting era, especially owing to the release of structural models by DeepMind's AlphaFold[39] as well as exponentially increased enumerable chemical libraries from the *REAL* space.[31] On the other hand, the high-performance computing power needed to physically dock every single molecule within the multi-millions to billions present in existing chemical libraries is an unaffordable computational cost to many organizations, especially for academia and small start-ups. Fortunately, with the recent and fast evolution and deployment of machine learning algorithms in the application of drug discovery, a full integration combining machine learning and traditional docking-based, exhaustive pose sampling process makes it possible to cost-effectively screen ultra large libraries within a few weeks' time at a reasonably affordable computational cost.

Here, we implemented the recently emerging approach from Schrödinger: Active learning/Glide for its potential use of ultra-large virtual screening to aid in inhibitor discovery targeting WLS, a key protein required for Wnt secretion and yet currently undrugged by small molecules. Seeking first-in-class chemotypes, ~500 million potential molecules were screened *in silico* against the identified druggable pocket for small molecule binding within the WLS transmembrane region. Applying a 50-CPU parallel job setting, we were able to complete the stage of Active Learning/Glide in only 6 days. The Glide SP re-scoring of the top 1 million ligands (predicted by the model trained from Active Learning) from the whole library took another 6 days using the same computing resources available within the Experimental Drug Development Center (EDDC) server. Upon the completion of the computational workflow, we focused on further hit selection process from the top 10,000 ranked compounds based on Glide SP scoring functions. Due to the lack of a co-crystal structure of a small molecule inhibitor bound to WLS, our hit prioritization was guided mainly by volume overlapping clustering followed by diversity-based selection. This method allowed us to shortlist multiple and diverse chemical scaffolds that aligned with our resources for follow-up compound purchase and experimental validation.

Encouragingly, our effort led to the identification of two hits out of the sixty-eight purchased compounds, resulting in a hit rate of nearly 3%, which is significantly higher than a traditional HTS campaign especially for a previously undrugged target (0.05–0.1% hit rate). ETC-450 and ETC-451 exhibited the dose-dependent inhibition of Wnt/β-catenin reporter activity with an IC_{50} of 6.3 μM and 7.7 μM, respectively. ETC-450 did not block WNT/WLS interaction, so did not undergo further biochemical characterization. Comparing the predicted binding pose of ETC-450 in the WLS druggable cavity (Figure S3B), its inhibitory activity could be very different from ETC-451. ETC-451 was further confirmed as a WLS inhibitor from a diverse array of cell-based assays. ETC-451 reduced Wnt target gene expression and colony formation in Wnt-addicted pancreatic cancer cells. Preliminary SAR for ETC-451 was established by testing 11 analogs that highlighted the role of the 2-aminomethyl on the core scaffold as a key moiety conferring inhibitory activity against WLS. As a hypothesis derived from molecular docking and MD simulations, the 2-aminomethyl interacted with Asp353 via an H-bond interaction. In accordance with predictions from modeling, mutating Asp353 to alanine rendered WLS drug-insensitive as demonstrated by the rescued STF activities in WLS-knockout cells. The biochemical results validated our modeling hypothesis and rationalized the importance of the 2-aminomethyl group from initial SAR. Nevertheless, the relatively high IC_{50}s of the hit compounds make it more challenging to perform any *in vivo* study using the compounds. We also observed off-target cytotoxicity when we used higher concentrations of the compounds. In addition, we noticed that the protein levels of WNT3A were frequently reduced after the treatment of the compounds, especially for ETC-451. We speculate that lipidated Wnt proteins might be prone to degradation when they are not bound to WLS. In contrast, WNTs will accumulate in the endoplasmic reticulum (ER) after PORCN inhibition since they are not acylated and hence may be more stable.

Our approach required some assumptions due to incomplete information. For example, we removed WNT8A from the complex structure of WLS-WNT8A and used the WLS structure alone for virtual screening. However, whether the native WLS apo-structure assumes the similar structural conformation as WLS-WNT8A remains unknown. As one test of this assumption, we compared the AlphaFold model of WLS in its

apo structural conformation with the experimentally determined cryo-EM structural complex. The overall alignment of the backbone Ca of the two structures showed a root-mean-square deviation (RMSD) of only 1.27 Å, suggesting our initial assumption was valid. However, the identified druggable binding site that we targeted was partially occluded in the apo-structure according to the AlphaFold model (data not shown). This finding was further confirmed by the publication of the apo-WLS structure recently.[40] Future computational screening based on the apo-structure of WLS may yield additional potent and structurally novel inhibitors.

In the current study, we only tested a tiny fraction of compounds from the top 10,000 ranked according to the Glide SP scoring function. This doesn't exclude the possibility that additional true active or more potent inhibitors are present within the list. From a computational perspective, it would be ideal to apply more extensive physics-based calculations such as absolute free energy perturbation (ABFE) to rescore a larger fraction of the compound pool for hit prioritization.[41] However, such calculations are computationally expensive and not readily available to us yet. Nevertheless, testing a significantly higher number of compounds beyond what has been evaluated here may potentially lead to the discovery of other novel WLS inhibitor chemotypes. To facilitate such discovery, we include here a dataset of the entire top 10,000 ranked compounds so that others may evaluate and follow up at their own discretion. Meanwhile, we are hopeful that a medicinal chemistry campaign centered on ETC-451 will develop the current hit into a more potent lead or tool compound suitable for further studies on WLS and Wnt biology. Finally, the mechanism of how ETC-450 engages WLS binding and inhibits the Wnt/β-catenin reporter activity warrants further investigation.

Limitations of the study

Our study has several limitations. The hits we describe are not yet optimized, and so their potency remains in the low micromolar range, and there are apparent off-target cytotoxic effects at higher concentrations. A second limitation is that, because the hits are not optimized, they cannot yet be tested in *in vivo* models. Third, despite several attempts, we have not yet determined the structure of ETC-451 in a complex with WLS to validate the docking predictions. Lastly, at the time of our structure-based virtual screening, there was no apo-WLS structure available and our work was performed by removing Wnt from the previously reported WLS-Wnt8A complex (PDB: 7KC4).

STAR★METHODS

Detailed methods are provided in the online version of this paper and include the following:

- KEY RESOURCES TABLE
- RESOURCE AVAILABILITY
  - Lead contact
  - Materials availability
  - Data and code availability
- EXPERIMENTAL MODEL AND STUDY PARTICIPANT DETAILS
- METHOD DETAILS
  - Identify druggable sites on WLS
  - Active Learning/Glide (Schrödinger version 2021-3)
  - Wnt/β-catenin reporter assay
  - Western blot
  - Immunoprecipitation
  - RNA analysis
  - Low-density colony formation assay
  - WLS functional assay
  - Molecular dynamic simulations
- QUANTIFICATION AND STATISTICAL ANALYSIS

SUPPLEMENTAL INFORMATION

Supplemental information can be found online at https://doi.org/10.1016/j.isci.2024.110454.

ACKNOWLEDGMENTS

This research was supported in part by the National Research Foundation Singapore and administered by the Ministry of Health's National Medical Research Council (NMRC) under Singapore Translational Research (STaR) Award MOH-000155 and USA NIH 5R01 CA275005 (to DMV), and EDDC innovation platform funding. Graphical abstract and Figure 1 was created with BioRender.

AUTHOR CONTRIBUTIONS

Conceptualization, W.X., T.H.K., J.C., and D.M.V.; investigation, J.Y., P.J.L., and W.X.; writing, J.Y., P.J.L., D.M.V, and W.X.; visualization, J.Y. and P.J.L.; supervision, D.M.V. and W.X.; funding, D.M.V. and W.X.

DECLARATION OF INTERESTS

W.X. is an employee of the Experimental Drug Development Center. This institute has a commercial interest in the development of ETC-159. D.M.V. also has financial interest in ETC-159. Other authors declare no competing interests.

Received: September 3, 2023
Revised: March 27, 2024
Accepted: July 2, 2024
Published: July 5, 2024

REFERENCES

1. Loh, K.M., Amerongen, R. van, and Nusse, R. (2016). Generating Cellular Diversity and Spatial Form: Wnt Signaling and the Evolution of Multicellular Animals. Dev. Cell *38*, 643–655. https://doi.org/10.1016/j.devcel.2016.08.011.
2. Nusse, R. (2012). Wnt Signaling. Cold Spring Harb. Perspect. Biol. *4*, a011163. https://doi.org/10.1101/cshperspect.a011163.
3. Teo, J.-L., and Kahn, M. (2010). The Wnt signaling pathway in cellular proliferation and differentiation: A tale of two coactivators. Adv. Drug Deliv. Rev. *62*, 1149–1155. https://doi.org/10.1016/j.addr.2010.09.012.
4. Zhong, Z., Yu, J., Virshup, D.M., and Madan, B. (2020). Wnts and the hallmarks of cancer. Cancer Metast. Rev. *39*, 625–645. https://doi.org/10.1007/s10555-020-09887-6.
5. Zhan, T., Rindtorff, N., and Boutros, M. (2017). Wnt signaling in cancer. Oncogene *36*, 1461–1473. https://doi.org/10.1038/onc.2016.304.
6. Ng, L.F., Kaur, P., Bunnag, N., Suresh, J., Sung, I.C.H., Tan, Q.H., Gruber, J., and Tolwinski, N.S. (2019). WNT Signaling in Disease. Cells *8*, 826. https://doi.org/10.3390/cells 8080826.
7. Takada, R., Satomi, Y., Kurata, T., Ueno, N., Norioka, S., Kondoh, H., Takao, T., and Takada, S. (2006). Monounsaturated Fatty Acid Modification of Wnt Protein: Its Role in Wnt Secretion. Dev. Cell *11*, 791–801. https://doi.org/10.1016/j.devcel.2006.10.003.
8. Janda, C.Y., Waghray, D., Levin, A.M., Thomas, C., and Garcia, K.C. (2012). Structural Basis of Wnt Recognition by Frizzled. Science *337*, 59–64. https://doi.org/10.1126/science.1222879.
9. Heuvel, M.V.D., Harryman-Samos, C., Klingensmith, J., Perrimon, N., and Nusse, R. (1993). Mutations in the segment polarity genes wingless and porcupine impair secretion of the wingless protein. EMBO J. *12*, 5293–5302. https://doi.org/10.1002/j.1460-2075.1993.tb06225.x.
10. Coombs, G.S., Yu, J., Canning, C.A., Veltri, C.A., Covey, T.M., Cheong, J.K., Utomo, V., Banerjee, N., Zhang, Z.H., Jadulco, R.C., et al. (2010). WLS-dependent secretion of WNT3A requires Ser209 acylation and vacuolar acidification. J. Cell Sci. *123*, 3357–3367. https://doi.org/10.1242/jcs.072132.
11. Bartscherer, K., Pelte, N., Ingelfinger, D., and Boutros, M. (2006). Secretion of Wnt ligands requires Evi, a conserved transmembrane protein. Cell *125*, 523–533. https://doi.org/10.1016/j.cell.2006.04.009.
12. Bänziger, C., Soldini, D., Schütt, C., Zipperlen, P., Hausmann, G., and Basler, K. (2006). Wntless, a conserved membrane protein dedicated to the secretion of Wnt proteins from signaling cells. Cell *125*, 509–522. https://doi.org/10.1016/j.cell.2006.02.049.
13. Gonsalves, F.C., Klein, K., Carson, B.B., Katz, S., Ekas, L.A., Evans, S., Nagourney, R., Cardozo, T., Brown, A.M.C., and Dasgupta, R. (2011). An RNAi-based chemical genetic screen identifies three small-molecule inhibitors of the Wnt/wingless signaling pathway. Proc Natl. Acad. Sci. USA *108*, 5954–5963. https://doi.org/10.1073/pnas.1017496108.
14. Emami, K.H., Nguyen, C., Ma, H., Kim, D.H., Jeong, K.W., Eguchi, M., Moon, R.T., Teo, J.-L., Oh, S.W., Kim, H.Y., et al. (2004). A small molecule inhibitor of beta-catenin/CREB-binding protein transcription [corrected]. Proc Natl. Acad. Sci. USA *101*, 12682–12687. https://doi.org/10.1073/pnas.0404875101.
15. Shah, K., Panchal, S., and Patel, B. (2021). Porcupine Inhibitors: Novel and Emerging Anti-cancer Therapeutics Targeting the Wnt Signaling Pathway. Pharmacol. Res. *167*, 105532. https://doi.org/10.1016/j.phrs.2021.105532.
16. Liu, J., Pan, S., Hsieh, M.H., Ng, N., Sun, F., Wang, T., Kasibhatla, S., Schuller, A.G., Li, A.G., Cheng, D., et al. (2013). Targeting Wnt-driven cancer through the inhibition of Porcupine by LGK 974. Proc Natl. Acad. Sci. USA *110*, 20224–20229. https://doi.org/10.1073/pnas.1314239110.
17. Madan, B., Ke, Z., Harmston, N., Ho, S.Y., Frois, A.O., Alam, J., Jeyaraj, D.A., Pendharkar, V., Ghosh, K., Virshup, I.H., et al. (2016). Wnt addiction of genetically defined cancers reversed by PORCN inhibition. Oncogene *35*, 2197–2207. https://doi.org/10.1038/onc.2015.280.
18. Zhong, Z., and Virshup, D.M. (2020). Wnt Signaling and Drug Resistance in Cancer. Mol. Pharmacol. *97*, 72–89. https://doi.org/10.1124/mol.119.117978.
19. Gurney, A., Axelrod, F., Bond, C.J., Cain, J., Chartier, C., Donigan, L., Fischer, M., Chaudhari, A., Ji, M., Kapoun, A.M., et al. (2012). Wnt pathway inhibition via the targeting of Frizzled receptors results in decreased growth and tumorigenicity of human tumors. Proc. Natl. Acad. Sci. USA *109*, 11717–11722. https://doi.org/10.1073/pnas.1120068109.
20. Pavlovic, Z., Adams, J.J., Blazer, L.L., Gakhal, A.K., Jarvik, N., Steinhart, Z., Robitaille, M., Mascall, K., Pan, J., Angers, S., et al. (2018). A synthetic anti-Frizzled antibody engineered for broadened specificity exhibits enhanced anti-tumor properties. mAbs *10*, 1157–1167. https://doi.org/10.1080/19420862.2018.1515 565.
21. Nygaard, R., Yu, J., Kim, J., Ross, D.R., Parisi, G., Clarke, O.B., Virshup, D.M., and Mancia, F. (2021). Structural Basis of WLS/Evi-Mediated Wnt Transport and Secretion. Cell *184*, 194–206.e14. https://doi.org/10.1016/j.cell.2020.11.038.
22. Zhong, Q., Zhao, Y., Ye, F., Xiao, Z., Huang, G., Xu, M., Zhang, Y., Zhan, X., Sun, K., Wang, Z., et al. (2021). Cryo-EM structure of human Wntless in complex with Wnt3a. Nat. Commun. *12*, 4541. https://doi.org/10.1038/s41467-021-24731-3.
23. Maestro (Schrödinger Release 2021-2). https://www.schrodinger.com/platform/products/maestro/
24. Leung, S.S.F., Sindhikara, D., and Jacobson, M.P. (2016). Simple Predictive Models of Passive Membrane Permeability Incorporating Size-Dependent Membrane-Water Partition. J. Chem. Inf. Model. *56*, 924–929. https://doi.org/10.1021/acs.jcim.6b00005.
25. Lyu, J., Wang, S., Balius, T.E., Singh, I., Levit, A., Moroz, Y.S., O'Meara, M.J., Che, T., Algaa, E., Tolmachova, K., et al. (2019). Ultra-large library docking for discovering new chemotypes. Nature *566*, 224–229. https://doi.org/10.1038/s41586-019-0917-9.
26. Gorgulla, C., Boeszoermenyi, A., Wang, Z.-F., Fischer, P.D., Coote, P.W., Das, K.M.P., Malets, Y.S., Radchenko, D.S., Moroz, Y.S., Scott, D.A., et al. (2020). An open-source drug discovery platform enables ultra-large virtual screens. Nature *580*, 663–668. https://doi.org/10.1038/s41586-020-2117-z.
27. Luttens, A., Gullberg, H., Abdurakhmanov, E., Vo, D.D., Akaberi, D., Talibov, V.O., Nekhotiaeva, N., Vangeel, L., Jonghe, S.D., Jochmans, D., et al. (2022). Ultralarge Virtual Screening Identifies SARS-CoV-2 Main Protease Inhibitors with Broad-Spectrum Activity against Coronaviruses. J. Am. Chem. Soc. *144*, 2905–2920. https://doi.org/10.1021/jacs.1c08402.
28. Sadybekov, A.A., Sadybekov, A.V., Liu, Y., Iliopoulos-Tsoutsouvas, C., Huang, X.-P., Pickett, J., Houser, B., Patel, N., Tran, N.K., Tong, F., et al. (2022). Synthon-based ligand discovery in virtual libraries of over 11 billion compounds. Nature *601*, 452–459. https://doi.org/10.1038/s41586-021-04220-9.
29. Friesner, R.A., Banks, J.L., Murphy, R.B., Halgren, T.A., Klicic, J.J., Mainz, D.T., Repasky, M.P., Knoll, E.H., Shelley, M., Perry, J.K., et al. (2004). Glide: a new approach for rapid, accurate docking and scoring. 1. Method and assessment of docking accuracy. J. Med. Chem. *47*, 1739–1749. https://doi.org/10.1021/jm0306430.
30. DeepChem Project https://deepchem.io.
31. Enamine (2020). REAL Space. https://enamine.net/library-synthesis/real-compounds/real-space-navigator.
32. Meijer, L., Skaltsounis, A.-L., Magiatis, P., Polychronopoulos, P., Knockaert, M., Leost, M., Ryan, X.P., Vonica, C.A., Brivanlou, A., Dajani, R., et al. (2003). GSK-3-Selective Inhibitors Derived from Tyrian Purple Indirubins. Chem. Biol. *10*, 1255–1266.

https://doi.org/10.1016/j.chembiol.2003.11.010.

33. Yu, J., Liao, P.J., Xu, W., Jones, J.R., Everman, D.B., Flanagan-Steet, H., Keller, T.H., and Virshup, D.M. (2021). Structural model of human PORCN illuminates disease-associated variants and drug-binding sites. J. Cell Sci. *134*, jcs259383. https://doi.org/10.1242/jcs.259383.
34. Liu, Y., Qi, X., Donnelly, L., Elghobashi-Meinhardt, N., Long, T., Zhou, R.W., Sun, Y., Wang, B., and Li, X. (2022). Mechanisms and inhibition of Porcupine-mediated Wnt acylation. Nature *607*, 816–822. https://doi.org/10.1038/s41586-022-04952-2.
35. Kaur, A., Lim, J.Y.S., Sepramaniam, S., Patnaik, S., Harmston, N., Lee, M.A., Petretto, E., Virshup, D.M., and Madan, B. (2021). WNT inhibition creates a BRCA -like state in Wnt-addicted cancer. EMBO Mol. Med. *13*, e13349. https://doi.org/10.15252/emmm.202013349.
36. Moti, N., Yu, J., Boncompain, G., Perez, F., and Virshup, D.M. (2019). Wnt traffic from endoplasmic reticulum to filopodia. PLoS One *14*, e0212711. https://doi.org/10.1371/journal.pone.0212711.
37. Kuntz, I.D., Blaney, J.M., Oatley, S.J., Langridge, R., and Ferrin, T.E. (1982). A geometric approach to macromolecule-ligand interactions. J. Mol. Biol. *161*, 269–288. https://doi.org/10.1016/0022-2836(82)90153-x.
38. Meng, X.-Y., Zhang, H.-X., Mezei, M., and Cui, M. (2011). Molecular Docking: A Powerful Approach for Structure-Based Drug Discovery. Curr. Comput. Aided Drug Des. *7*, 146–157. https://doi.org/10.2174/157340911795677602.
39. Jumper, J., Evans, R., Pritzel, A., Green, T., Figurnov, M., Ronneberger, O., Tunyasuvunakool, K., Bates, R., Žídek, A., Potapenko, A., et al. (2021). Highly accurate protein structure prediction with AlphaFold. Nature *596*, 583–589. https://doi.org/10.1038/s41586-021-03819-2.
40. Qi, X., Hu, Q., Elghobashi-Meinhardt, N., Long, T., Chen, H., and Li, X. (2023). Molecular basis of Wnt biogenesis, secretion, and Wnt7-specific signaling. Cell *186*, 5028–5040.e14. https://doi.org/10.1016/j.cell.2023.09.021.
41. Cournia, Z., Allen, B.K., Beuming, T., Pearlman, D.A., Radak, B.K., and Sherman, W. (2020). Rigorous Free Energy Simulations in Virtual Screening. J. Chem. Inf. Model. *60*, 4153–4169. https://doi.org/10.1021/acs.jcim.0c00116.
42. Xu, Q., Wang, Y., Dabdoub, A., Smallwood, P.M., Williams, J., Woods, C., Kelley, M.W., Jiang, L., Tasman, W., Zhang, K., and Nathans, J. (2004). Vascular Development in the Retina and Inner Ear Control by Norrin and Frizzled-4, a High-Affinity Ligand-Receptor Pair. Cell *116*, 883–895. https://doi.org/10.1016/s0092-8674(04)00216-8.
43. McCulloch, M.W., Coombs, G.S., Banerjee, N., Bugni, T.S., Cannon, K.M., Harper, M.K., Veltri, C.A., Virshup, D.M., and Ireland, C.M. (2009). Psammaplin A as a general activator of cell-based signaling assays via HDAC inhibition and studies on some bromotyrosine derivatives. Bioorg. Med. Chem. *17*, 2189–2198. https://doi.org/10.1016/j.bmc.2008.10.077.
44. Willert, K., Brown, J.D., Danenberg, E., Duncan, A.W., Weissman, I.L., Reya, T., Yates, J.R. 3rd., and Nusse, R. (2003). Wnt proteins are lipid-modified and can act as stem cell growth factors. Nature *423*, 448–452. https://doi.org/10.1038/nature01611.
45. Tanaka, K., Okabayashi, K., Asashima, M., Perrimon, N., and Kadowaki, T. (2000). The evolutionarily conserved porcupine gene family is involved in the processing of the Wnt family. Eur. J. Biochem. *267*, 4300–4311. https://doi.org/10.1046/j.1432-1033.2000.01478.x.
46. Veeman, M.T., Slusarski, D.C., Kaykas, A., Louie, S.H., and Moon, R.T. (2003). Zebrafish prickle, a modulator of noncanonical Wnt/Fz signaling, regulates gastrulation movements. Curr. Biol. *13*, 680–685. https://doi.org/10.1016/s0960-9822(03)00240-9.
47. REAL database subsets https://enamine.net/compound-collections/real-compounds/real-database-subsets.
48. Yu, J., Yusoff, P.A.M., Woutersen, D.T.J., Goh, P., Harmston, N., Smits, R., Epstein, D.M., Virshup, D.M., and Madan, B. (2020). The Functional Landscape of Patient-Derived RNF43 Mutations Predicts Sensitivity to Wnt Inhibition. Cancer Res. *80*, 5619–5632. https://doi.org/10.1158/0008-5472.can-20-0957.

STAR★METHODS

KEY RESOURCES TABLE

REAGENT or RESOURCE	SOURCE	IDENTIFIER
Antibodies		
Anti-Wnt3A	Takada et al.[7]	RRID: AB_3106914
Anti-V5 tag (clone SV5-Pk1)	BioRad	Cat#MCA1360; RRID:AB_322378
Anti-HA tag (C29F4)	Cell Signaling Technology	Cat#3724; RRID:AB_1549585
Anti-β-tubulin (Ep1569y)	Abcam	Cat#ab52623; RRID:AB_869991
Chemicals, peptides, and recombinant proteins		
ETC-159	Madan et al.[17]	ETC-1922159
ETC-450	Enamine	Z3550507351
ETC-450A	Enamine	Z3551028149
ETC-451	Enamine	Z4065386141
ETC-451A	Enamine	Z3828272328
Fetal bovine serum (FBS)	Thermo Fisher Scientific	Cat#16000044
Penicillin-Streptomycin	Thermo Fisher Scientific	Cat#15140122
Sodium pyruvate	Lonza	Cat#13-115E
DMEM (High Glucose)	Nacalai tesque	Cat#08459-64
Insulin	Gibco	Cat#41400-045
Lipofectamine 2000	Thermo Fisher Scientific	Cat#11668019
Opti-MEM® I reduced serum medium	Thermo Fisher Scientific	Cat#51985-034
EDTA-free cOmplete protease inhibitor cocktail	Roche	Cat#11873580001
Amersham ECL western blotting detection reagent	Cytiva	Cat#RPN2105
A/G plus agarose	Santa Cruz	Cat#sc2003
Crystal violet	Sigma	Cat#C0775
Critical commercial assays		
Luciferase Assay System	Promega	Cat#1501
RNeasy mini kit	Qiagen	Cat#74104
BlitzAMP RT kit	Mirxes	Cat#1203103
BlizAMP Hotstart qPCR Master Mix	Mirxes	Cat#1204202
Pierce BCA protein assay kit	Thermo Fisher Scientific	Cat#23227
Deposited data		
REAL database subsets	Enamine	https://enamine.net/compound-collections/real-compounds/real-database-subsets
The top 10,000 ranked hits from our virtual screening for drugging WLS		https://dataverse.harvard.edu/dataset.xhtml?persistentId=doi:10.7910/DVN/UNCDH9
Experimental models: Cell lines		
STF reporter cells	Xu et al.[42]	N/A
STF3a cells	McCulloch et al.[43]	N/A
HPAF-II cells	ATCC	CRL-1997
PANC 08.13 cells	ATCC	CRL-2551
WLS knockout RKO cells	Moti et al.[36]	N/A

(*Continued on next page*)

Continued

REAGENT or RESOURCE	SOURCE	IDENTIFIER
Oligonucleotides		
Primer for qRT-PCR assay	IDT	Table S3
Recombinant DNA		
pPGK-mWnt3a	Willert et al.[44]	N/A
pCS2+-3xFlag-hWLSv1	Nygaard et al.[21]	N/A
pCS2+-3xFlag-hWLSv1 D353A	This paper	N/A
pMKIT-3xHA-mPORCN-D	Tanaka et al.[45]	N/A
Super TOPFlash report	Veeman et al.[46]	RRID:Addgene_12456
Software and algorithms		
Maestro	Schrödinger version 2021-2	https://www.schrodinger.com/platform/products/maestro/
Sitemap	Schrödinger version 2021-2	https://www.schrodinger.com/platform/products/sitemap/
Active Learning/Glide	Schrödinger version 2021-3	https://www.schrodinger.com/platform/products/glide/
Desmond Molecular Dynamics System	D.E. Shaw Research	https://www.schrodinger.com/platform/products/desmond/
DeepChem 2022	DeepChem	https://deepchem.io
Pymol 3.0	Pymol	https://www.pymol.org/
Prism 10	GraphPad	https://www.graphpad.com/
BioRender	BioRender	https://app.biorender.com/

RESOURCE AVAILABILITY

Lead contact

Further information or requests for resources should be directed to the lead contact, Weijun Xu: xu_weijun@eddc.sg.

Materials availability

This study did not generate any new unique reagents. The small molecule inhibitors can be ordered for synthesis through Enemine website (https://enamine.net/). Plasmids and associated vector maps generated in this study are available upon request. Any additional material information for this work is available from the lead contact upon request.

Data and code availability

- The top 10,000 ranked hits from our virtual screening for drugging WLS are publicly available as the link: https://dataverse.harvard.edu/dataset.xhtml?persistentId=doi:10.7910/DVN/UNCDH9.
- This paper does not report original code.
- Any additional information required to analyze the data in this paper is available from the lead contact upon request.

EXPERIMENTAL MODEL AND STUDY PARTICIPANT DETAILS

STF reporter cell line (human embryonic kidney HEK293 with stably expressing firefly luciferase gene under the control of eight tandem repeats of the TOPFlash TCF/LEF responsive promoter element) was a gift from Kang Zhang (University of California San Diego, La Jolla, CA).[42] STF3A cell line was described previously.[10] Mycoplasma test was performed regularly using MycoAlert Mycoplasma detection kit (Lonza). STF cells were cultured in Dulbecco's modified Eagle medium supplemented with 10% fetal bovine serum (FBS), penicillin/streptomycin, and sodium pyruvate. HPAF-II cells were cultured in EMEM medium supplemented with 10% fetal bovine serum (FBS), L-glutamate, penicillin/streptomycin. PANC 08.13 cells were cultured in RPMI-1640 medium supplemented with 15% FBS, L-glutamate, penicillin/streptomycin, sodium pyruvate and insulin. The cells were passaged every 3 to 4 days and used for experiments before passage number 20.

METHOD DETAILS

Identify druggable sites on WLS

The cryo-EM structure of WLS bound to WNT8A (PDB: 7KC4) was downloaded and prepared using the Protein Preparation Workflow using default settings within Maestro.[23] Schrödinger Sitemap calculations identified a potential druggable site (DScore 1.18) within the transmembrane tunnel of WLS. For molecular docking and virtual screen, the grid generation was performed by centring the inner box around residue Leu349.

Active Learning/Glide (Schrödinger version 2021-3)

The Enamine 350/3 database, which contains >500 million compounds with the most stringent physicochemical profiles and a high potency for optimization (270 ≤ MW ≤ 350, 14 ≤ heavy atoms ≤ 26, SlogP ≤ 3, and aryl rings ≤ 2) and with pan-assay interfering compounds (PAINS) and toxic compounds pre-removed, was used for virtual screening.[47] Ligands were prepared at pH 7.4 with maximal 16 stereoisomer generations. During the process of Active learning/Glide screening, 3 iterations of molecular docking followed by machine learning were implemented. In the initial iteration, 50K diverse compounds from the entire library were chosen for Glide SP docking. After the docking was completed, machine learning training and validation were performed using the DeepChem module (Schrödinger). Next, the whole library was evaluated by the model to predict the top 50K compounds for their docking scores and feedback to the original 50K compound dataset. From here, the total number of 100K compounds was subjected to a new round of Glide SP docking, machine learning, and evaluation. The process is repeated for 3 iterations and once completed, the trained model predicted a final list of the top 1 million compound set that likely would have best docking scores and the whole dataset was re-docked by Glide and re-scored by Glide SP scoring function. The calculation was performed using 50 CPUs on the Glide server available at EDDC.

Wnt/β-catenin reporter assay

Reporter assays were performed as previously described.[48] Briefly, STF3A cells were treated with varying concentrations of compounds for 48 h. Cells were lysed in Reporter Lysis Buffer (Promega) containing protease inhibitors. STF reporter activity was measured using firefly luciferase substrate (Promega) and was normalized to the cell viability, determined using LDH assay.[10] For STF cells cultured with WNT3A conditioned media, WNT3A-conditioned medium was obtained from STF3A cells stably expressing WNT3A and added to STF cells with varying concentrations of compounds. Luciferase activity was validated after 48 h treatment.

For WLS rescue experiments, STF cells were transfected in 24 well plates with 10 ng WNT3A expression plasmid, 50 ng mCherry, and 50 ng 3xFlag-hWLSv1 or 3xHA-mPORCN-D expression plasmids using Lipofectamine 2000 (Thermo Fisher Scientific). Compounds were added 6 h after transfection and the cells were treated for 48 h. Luciferase activity was quantitated and normalized to the mCherry reading (excitation 580 nm and emission 610 nm) as cell viability.

Western blot

To monitor Wnt secretion into the culture medium, STF3A cells were grown in 12 well plates and treated with compounds for 48 h with low serum media (2% FBS). Medium was collected and subjected to western blot analysis. Cells were lysed with RIPA buffer: 50 mM Tris (ph 7.4), 150 mM NaCl, 1% NP-40, 0.1% sodium deoxycholate, 1 mM EDTA and protease inhibitor cocktail (Merck). Antibody against WNT3A was a gift from Shinji Takada (National Institutes of Nature Sciences, Okazaki, Japan) as mouse hybridoma supernatant and used at 1:100 dilution. β-tubulin (Ep1569y) rabbit monoclonal antibody was from Abcam and used at 1:2000 dilution. Anti-HA tag rabbit monoclonal antibody (C29F4) was from Cell Signaling Technology (#3724) and used at 1:1000 dilution. Immunoblots on PVDF were developed using Amersham ECL western blotting detection reagent (Cytiva). The images were captured using the Chemidoc Touch (BioRad).

Immunoprecipitation

Cells grown in 6-well plates and transfected with 200 ng of WNT3A expression plasmid along with 200 ng of expression plasmid encoding WLS-V5 or 3xHA-tagged PORCN using Lipofectamine 2000. Six hrs after transfection, the medium was changed with compounds in complete media. Cells were lysed with HEPES buffer after 48 h culturing with compounds: 50 mM HEPES (pH 7.4), 150 mM NaCl, 1 mM EDTA, 0.6% NP40, 1 mM DTT and protease inhibitor cocktail (Sigma). 1 μg of anti-V5 tag mouse monoclonal antibody (Bio-Rad) was added to 500 μg of total protein lysates for 16 h in the cold room with tumbling. 40 μL of protein A/G plus agarose (#sc-2003, Santa Cruz) was added the next day and incubated for another 2 h before washing and elution.

RNA analysis

Total RNA isolated from cell lines using RNeasy mini kit (Qiagen) was reverse transcribed into cDNA with BlitzAMP RT kit (Mirxes). Real-time quantitative PCR was performed with Mirxes BlizAMP Hotstart qPCR Master Mix on BioRad CFX96 real-time cycling machine. TATA binding protein (TBP) was used as a housekeeping gene. The qRT-PCR primers are listed in Table S3.

Low-density colony formation assay

HPAF-II and PANC 08.13 cells were plated in 48-well plates. 5,000 cells were seeded per well and cultured with compounds with varying concentrations in 1 mL complete culture media. The cells were allowed to form colonies and grow for 2–3 weeks. The colonies were fixed with ice-cold methanol and stained with crystal violet (0.5% CV in 25% methanol) (Sigma). After images were obtained, colonies were solubilized with 1% SDS, and the O.D at 590 nM was measured.

WLS functional assay

Site-directed mutagenesis was performed to generate mutant WLS expression constructs. Mutations were verified by Sanger sequencing. WLS knockout RKO cells were generated as described previously.[36] For the experimental procedure, cells were cultured in 24-well plates and then transfected with 200 ng of SuperTOPFlash plasmid, along with 100 ng of mCherry, 25 ng of WNT3A, and 5 ng of WLS expression

plasmids, using Lipofectamine 2000 (Thermo Fisher Scientific). After 6 h of transfection, the medium was replaced with or without a specific compound. Following an additional 24 h of incubation, the cells were harvested to measure luciferase activity.

Molecular dynamic simulations

MD simulations were performed with Desmond Molecular Dynamics System (D.E. Shaw Research) and associated analysis tools available within the Schrödinger suite (version 2022-2). The model system was set up with the 'system builder' utility to embed the transmembrane bundle of WLS in POPC lipids, whereas the OPLS-AA/2005 force-field parameters were implemented during simulations. The whole system was solvated in an orthorhombic box with solvent buffers of 10 Å along each dimension. The TIP3P solvent model was used to describe water molecules. Overall neutralization of the system was achieved by adding sodium and chloride ions at a physiological concentration of 0.15 M. The prepared model systems were then relaxed with a multistep default membrane protocol simulation protocol in Desmond. After the relaxation step, the whole system was subjected to a 1 *u*s molecular dynamic simulation. The SHAKE algorithm was used to constrain the bond length of hydrogen atoms. Long-range electrostatic forces were calculated with the particle-mesh Ewald (PME) method. The cutoff distance for computing short-range electrostatics and Lennard–Jones interaction was set to 9.0 Å. The trajectories were recorded every 5000 ps. MD simulations were performed with the NVIDIA QUODRO RTX6000 GPU card on a Linux station at the Experimental Drug Development Centre, Singapore.

QUANTIFICATION AND STATISTICAL ANALYSIS

Western blots were visualized and quantified on ImageLab 6.1 (Bio-Rad). Statistical analysis was performed using GraphPad. Statistical significance was calculated by Mann–Whitney unpaired 2-tailed t-test, and p-value of <0.05 was considered a significant difference.